eLIFE elifesciences.org

SHORT REPORT

The eukaryotic bell-shaped temporal rate of DNA replication origin firing emanates from a balance between origin activation and passivation

Jean-Michel Arbona[1], Arach Goldar[2], Olivier Hyrien[3], Alain Arneodo[4], Benjamin Audit[1]*

[1]Laboratoire de Physique, Université de Lyon, Ens de Lyon, Université Claude Bernard Lyon 1, CNRS , Lyon, France; [2]Ibitec-S, CEA, Gif-sur-Yvette, France; [3]Institut de Biologie de l'Ecole Normale Supérieure, Ecole Normale Supérieure, CNRS, INSERM, PSL Research University, Paris, France; [4]LOMA, Univ de Bordeaux, CNRS, UMR 5798, Talence, France

Abstract The time-dependent rate $I(t)$ of origin firing per length of unreplicated DNA presents a universal bell shape in eukaryotes that has been interpreted as the result of a complex time-evolving interaction between origins and limiting firing factors. Here, we show that a normal diffusion of replication fork components towards localized potential replication origins (*p-oris*) can more simply account for the $I(t)$ universal bell shape, as a consequence of a competition between the origin firing time and the time needed to replicate DNA separating two neighboring *p-oris*. We predict the $I(t)$ maximal value to be the product of the replication fork speed with the squared *p-ori* density. We show that this relation is robustly observed in simulations and in experimental data for several eukaryotes. Our work underlines that fork-component recycling and potential origins localization are sufficient spatial ingredients to explain the universality of DNA replication kinetics.
DOI: https://doi.org/10.7554/eLife.35192.001

***For correspondence:** benjamin.audit@ens-lyon.fr

Competing interests: The authors declare that no competing interests exist.

Funding: See page 10

Received: 18 January 2018
Accepted: 31 May 2018
Published: 01 June 2018

Reviewing editor: Bruce Stillman, Cold Spring Harbor Laboratory, United States

Introduction

Eukaryotic DNA replication is a stochastic process (***Hyrien et al., 2013***; ***Hawkins et al., 2013***; ***Hyrien, 2016b***). Prior to entering the S(ynthesis)-phase of the cell cycle, a number of DNA loci called potential origins (*p-oris*) are *licensed* for DNA replication initiation (***Machida et al., 2005***; ***Hyrien et al., 2013***; ***Hawkins et al., 2013***). During S-phase, in response to the presence of origin *firing* factors, pairs of replication *forks* performing bi-directional DNA synthesis will start from a subset of the *p-oris*, the active replication origins for that cell cycle (***Machida et al., 2005***; ***Hyrien et al., 2013***; ***Hawkins et al., 2013***). Note that the inactivation of *p-oris* by the passing of a replication fork called origin *passivation*, forbids origin firing in already replicated regions (***de Moura et al., 2010***; ***Hyrien and Goldar, 2010***; ***Yang et al., 2010***). The time-dependent rate of origin firing per length of unreplicated DNA, $I(t)$, is a fundamental parameter of DNA replication kinetics. $I(t)$ curves present a universal bell shape in eukaryotes (***Goldar et al., 2009***), increasing toward a maximum after mid-S-phase and decreasing to zero at the end of S-phase. An increasing $I(t)$ results in a tight dispersion of replication ending times, which provides a solution to the random completion problem (***Hyrien et al., 2003***; ***Bechhoefer and Marshall, 2007***; ***Yang and Bechhoefer, 2008***).

Models of replication in *Xenopus* embryo (***Goldar et al., 2008***; ***Gauthier and Bechhoefer, 2009***) proposed that the initial $I(t)$ increase reflects the progressive import during S-phase of a limiting origin firing factor and its recycling after release upon forks merge. The $I(t)$ increase was also

eLife digest Before a cell can divide, it must duplicate its DNA. In eukaryotes – organisms such as animals and fungi, which store their DNA in the cell's nucleus – DNA replication starts at specific sites in the genome called replication origins. At each origin sits a protein complex that will activate when it randomly captures an activating protein that diffuses within the nucleus. Once a replication origin activates or "fires", the complex then splits into two new complexes that move away from each other as they duplicate the DNA. If an active complex collides with an inactive one at another origin, the latter is inactivated – a phenomenon known as origin passivation. When two active complexes meet, they release the activating proteins, which diffuse away and eventually activate other origins in unreplicated DNA.

The number of origins that activate each minute divided by the length of unreplicated DNA is referred to as the "rate of origin firing". In all eukaryotes, this rate – also known as *I(t)* – follows the same pattern. First, it increases until more than half of the DNA is duplicated. Then it decreases until everything is duplicated. This means that, if plotted out, the graph of origin firing rate would always be a bell-shaped curve, even for organisms with genomes of different sizes that have different numbers of origins. The reason for this universal shape remained unclear.

Scientists had tried to create numerical simulations that model the rate of origin firing. However, for these simulations to reproduce the bell-shape curve, a number of untested assumptions had to be made about how DNA replication takes place. In addition, these models ignored the fact that it takes time to replicate the DNA between origins.

To take this time into account, Arbona et al. instead decided to model the replication origins as discrete and distinct entities. This way of building the mathematical model succeeded in reproducing the universal bell curve shape without additional assumptions. With this simulation, the balance between origin activation and passivation is enough to achieve the observed pattern.

The new model also predicts that the maximum rate of origin firing is determined by the speed of DNA replication and the density of origins in the genome. Arbona et al. verified this prediction in yeast, fly, frog and human cells – organisms with different sized genomes that take between 20 minutes and 8 hours to replicate their DNA. Lastly, the prediction also held true in yeast treated with hydroxyurea, an anticancer drug that slows DNA replication.

A better understanding of DNA replication can help scientists to understand how this process is perturbed in cancers and how drugs that target DNA replication can treat these diseases. Future work will explore how the 3D organization of the genome affects the diffusion of activating proteins within the cell nucleus.

DOI: https://doi.org/10.7554/eLife.35192.002

reproduced in a simulation of human genome replication timing that used a constant number of firing factors having an increasing reactivity through S-phase (**Gindin et al., 2014**). In these three models, an additional mechanism was required to explain the final $I(t)$ decrease by either a subdiffusive motion of the firing factor (**Gauthier and Bechhoefer, 2009**), a dependency of firing factors' affinity for *p-oris* on replication fork density (**Goldar et al., 2008**), or an inhomogeneous firing probability profile (**Gindin et al., 2014**). Here, we show that when taking into account that *p-oris* are distributed at a finite number of localized sites then it is possible to reproduce the universal bell shape of the $I(t)$ curves without any additional hypotheses than recycling of fork components. $I(t)$ increases following an increase of fork mergers, each merger releasing a firing factor that was trapped on DNA. Then $I(t)$ decreases due to a competition between the time t_c to fire an origin and the time t_r to replicate DNA separating two neighboring *p-ori*. We will show that when t_c becomes smaller than t_r, *p-ori* density over unreplicated DNA decreases, and so does $I(t)$. Modeling random localization of active origins in *Xenopus* embryo by assuming that every site is a (weak) *p-ori*, previous work implicitly assumed t_r to be close to zero (**Goldar et al., 2008**; **Gauthier and Bechhoefer, 2009**) forbidding the observation of a decreasing $I(t)$. Licensing of a limited number of sites as *p-ori* thus appears to be a critical property contributing to the observed canceling of $I(t)$ at the end of S-phase in all studied eukaryotes.

Results

Emergence of a bell-shaped $I(t)$

In our modeling of replication kinetics, a bimolecular reaction between a diffusing firing factor and a *p-ori* results in an origin firing event; then each half of the diffusing element is trapped and travels with a replication fork until two converging forks merge (termination, ***Figure 1a***). A molecular mechanism explaining the synchronous recruitment of firing factors to both replication forks was recently proposed (***Araki, 2016***), supporting the bimolecular scenario for *p-ori* activation. Under the assumption of a well-mixed system, for every time step dt, we consider each interaction between the $N_{FD}(t)$ free diffusing firing factors and the $N_{\mathrm{p-ori}}(t)$ *p-oris* as potentially leading to a firing with a probability $k_{on}dt$. The resulting simulated firing rate per length of unreplicated DNA is then:

$$I_S(t) = \frac{N_{fired}(t, t+dt)}{L_{unrepDNA}(t)dt}, \tag{1}$$

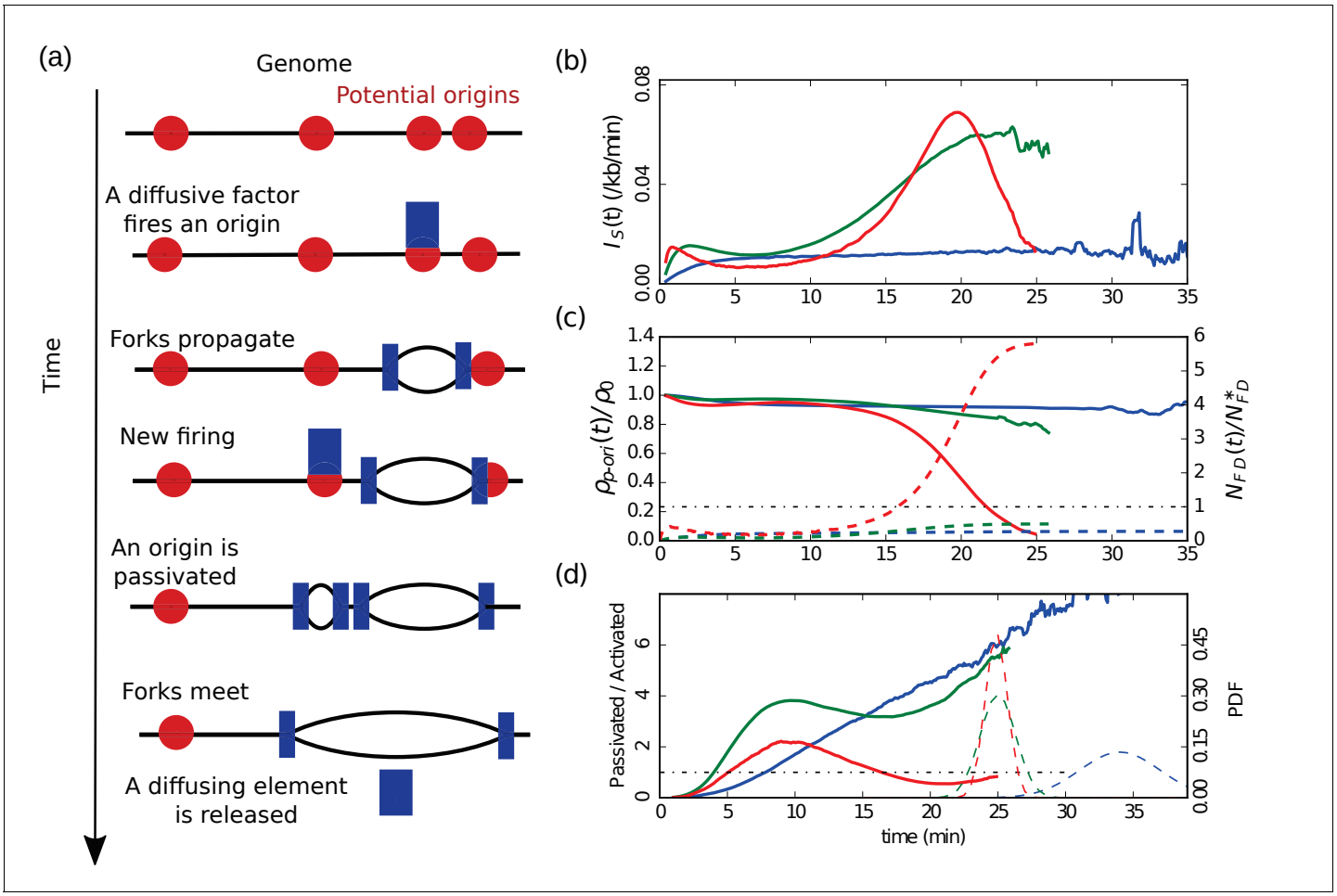

Figure 1. Emergence of a bell-shaped $I(t)$. (**a**) Sketch of the different steps of our modeling of replication initiation and propagation. (**b**) $I_S(t)$ (***Equation 1***) obtained from numerical simulations (Materials and methods) of one chromosome of length 3000 kb, with a fork speed $v = 0.6$ kb/min. The firing factors are loaded with a characteristic time of 3 min. From blue to green to red the interaction is increased and the number of firing factors is decreased: blue ($k_{on} = 5 \times 10^{-5}$ min^{-1}, $N_D^T = 1000$, $\rho_0 = 0.3$ kb^{-1}), green ($k_{on} = 6 \times 10^{-4}$ min^{-1}, $N_D^T = 250$, $\rho_0 = 0.5$ kb^{-1}), red ($k_{on} = 6 \times 10^{-3}$ min^{-1}, $N_D^T = 165$, $\rho_0 = 0.28$ kb^{-1}). (**c**) Corresponding normalized densities of *p-oris* (solid lines), and corresponding normalized numbers of free diffusing firing factors (dashed line): blue ($N^*_{FD} = 3360$), green ($N^*_{FD} = 280$), red ($N^*_{FD} = 28$); the horizontal dotted-dashed line corresponds to the critical threshold value $N_{FD}(t) = N^*_{FD}$. (**d**) Corresponding number of passivated origins over the number of activated origins (solid lines). Corresponding probability distribution functions (PDF) of replication time (dashed lines).

DOI: https://doi.org/10.7554/eLife.35192.003

where $N_{fired}(t,t+dt)$ is the number of *p-oris* fired between times t and $t+dt$, and $L_{unrepDNA}(t)$ is the length of unreplicated DNA a time t. Then we propagate the forks along the chromosome with a constant speed v, and if two forks meet, the two half firing complexes are released and rapidly reform an active firing factor. Finally, we simulate the chromosomes as 1D chains where prior to entering S-phase, the *p-oris* are precisely localized. For *Xenopus* embryo, the *p-ori* positions are randomly sampled, so that each simulated S-phase corresponds to a different positioning of the *p-oris*. We compare results obtained with periodic or uniform *p-ori* distributions (Materials and methods). For *S. cerevisiae*, the *p-ori* positions, identical for each simulation, are taken from the OriDB database (**Siow et al., 2012**). As previously simulated in human (**Löb et al., 2016**), we model the entry in S-phase using an exponentially relaxed loading of the firing factors with a time scale shorter than the S-phase duration T_{phase} (3 min for *Xenopus* embryo, where $T_{phase}\sim 30$ min, and 10 min for *S. cerevisiae*, where $T_{phase}\sim 60$ mins). After the short loading time, the total number of firing factors N_D^T is constant. As shown in **Figure 1b** (see also **Figure 2**), the universal bell shape of the $I(t)$ curves (**Goldar et al., 2009**) spontaneously emerges from our model when going from weak to strong interaction, and decreasing the number of firing factors below the number of *p-oris*. The details of the firing factor loading dynamics do not affect the emergence of a bell shaped $I(t)$, even though it can modulate its precise shape, especially early in S-phase.

In a simple bimolecular context, the rate of origin firing is $i(t)=k_{on}N_{\mathrm{p-ori}}(t)N_{FD}(t)$. The firing rate by element of unreplicated DNA is then given by

$$I(t)=k_{on}N_{FD}(t)\rho_{\mathrm{p-ori}}(t)\,, \tag{2}$$

where $\rho_{\mathrm{p-ori}}(t)=N_{\mathrm{p-ori}}(t)/L_{unrepDNA}(t)$. In the case of a strong interaction and a limited number of firing factors, all the diffusing factors react rapidly after loading and $N_{FD}(t)$ is small (**Figure 1 (c)**, dashed curves). Then follows a stationary phase where as long as the number of *p-oris* is high (**Figure 1 (c)**, solid curves), once a diffusing factor is released by the encounter of two forks, it reacts rapidly, and so $N_{FD}(t)$ stays small. Then, when the rate of fork mergers increases due to the fact that there are as many active forks but a smaller length of unreplicated DNA, the number of free firing factors increases up to N_D^T at the end of S-phase. As a consequence, the contribution of $N_{FD}(t)$ to $I(t)$ in **Equation (2)** can only account for a monotonous increase during the S phase. For $I(t)$ to reach a maximum I_{max} before the end of S-phase, we thus need that $\rho_{\mathrm{p-ori}}(t)$ decreases in the late S-phase. This happens if the time to fire a *p-ori* is shorter than the time to replicate a typical distance between two neighboring *p-oris*. The characteristic time to fire a *p-ori* is $t_c=1/k_{on}N_{FD}(t)$. The mean time for a fork to replicate DNA between two neighboring *p-oris* is $t_r=d(t)/v$, where $d(t)$ is the mean distance between unreplicated *p-oris* at time t. So the density of origins is constant as long as:

$$\frac{d(t)}{v}<\frac{1}{k_{on}N_{FD}(t)}\,, \tag{3}$$

or

$$N_{FD}(t)<N_{FD}^{\star}=\frac{v}{k_{on}d(t)}\,. \tag{4}$$

Thus, at the beginning of the S-phase, $N_{FD}(t)$ is small, $\rho_{\mathrm{p-ori}}(t)$ is constant (**Figure 1 (c)**, solid curves) and so $I_S(t)$ stays small. When $N_{FD}(t)$ starts increasing, as long as **Equation (4)** stays valid, $I_S(t)$ keeps increasing. When $N_{FD}(t)$ becomes too large and exceeds $N_{FD}^{\star}$, then **Equation (4)** is violated and the number of *p-oris* decreases at a higher rate than the length of unreplicated DNA, and $\rho_{\mathrm{p-ori}}(t)$ decreases and goes to zero (**Figure 1 (c)**, red solid curve). As $N_{FD}(t)$ tends to N_D^T, $I_S(t)$ goes to zero, and its global behavior is a bell shape (**Figure 1 (b)**, red). Let us note that if we decrease the interaction strength (k_{on}), then the critical $N_{FD}^{\star}$ will increase beyond N_D^T (**Figure 1 (c)**, dashed blue and green curves). $I_S(t)$ then monotonously increase to reach a plateau (**Figure 1 (b)**, green), or if we decrease further k_{on}, $I_S(t)$ present a very slow increasing behavior during the S-phase (**Figure 1 (b)**, blue). Now if we come back to strong interactions and increase the number of firing factors, almost all the *p-oris* are fired immediately and $I_S(t)$ drops to zero after firing the last *p-ori*.

Another way to look at the density of *p-oris* is to compute the ratio of the number of passivated origins by the number of activated origins (**Figure 1 (d)**). After the initial loading of firing factors,

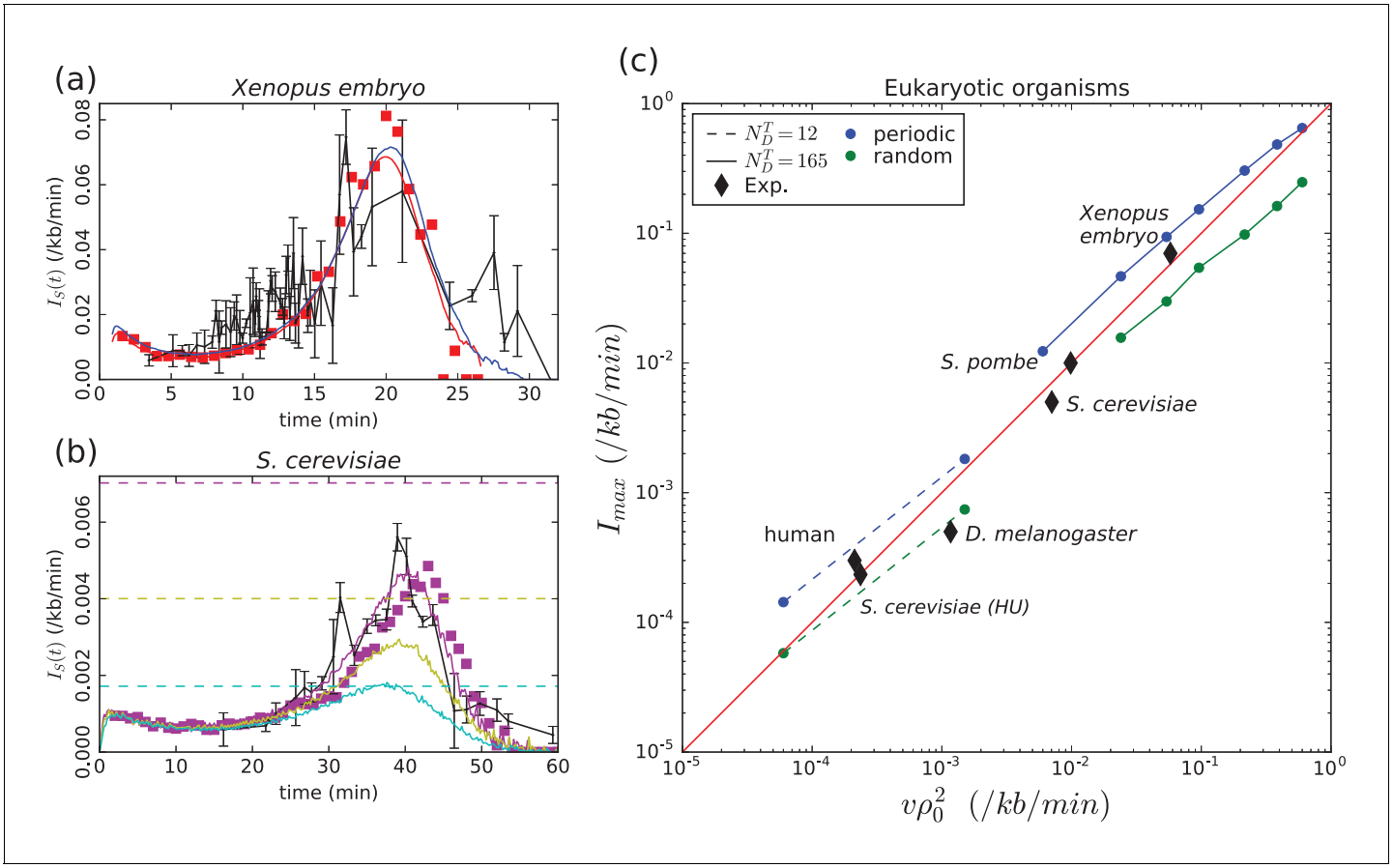

Figure 2. Model validation by experimental data. (**a**) *Xenopus* embryo: Simulated $I_S(t)$ (***Equation (1)***, Materials and methods) for a chromosome of length $L = 3000$ kb and a uniform distribution of *p-oris* (blue: $v = 0.6$ kb/min, $k_{on} = 3. \times 10^{-3}$ min^{-1}, $N_D^T = 187$, $\rho_0 = 0.70$ kb^{-1}) or a periodic distribution of *p-oris* (red: $v = 0.6$ kb/min, $k_{on} = 6 \times 10^{-3}$ min^{-1}, $N_D^T = 165$, $\rho_0 = 0.28$ kb^{-1}); (red squares) 3D simulations with the same parameter values as for periodic *p-ori* distribution; (black) experimental $I(t)$: raw data obtained from ***Goldar et al. (2009)*** were binned in groups of 4 data points; the mean value and standard error of the mean of each bin were represented. (**b**) *S. cerevisiae*: Simulated $I_S(t)$ (Materials and methods) for the 16 chromosomes with the following parameter values: $v = 1.5$ kb/min, $N_D^T = 143$, $k_{on} = 3.6 \times 10^{-3}$ min^{-1}, when considering only Confirmed origins (light blue), Confirmed and Likely origins (yellow) and Confirmed, Likely and Dubious origins (purple); the horizontal dashed lines mark the corresponding predictions for I_{max} (***Equation 5***); (purple squares) 3D simulations with the same parameter values considering Confirmed, Likely and Dubious origins; (black) experimental $I(t)$ from ***Goldar et al. (2009)***. (**c**) *Eukaryotic organisms:* I_{max} as a function of $v\rho_0^2$; (squares and bullets) simulations performed for regularly spaced origins (blue) and uniformly distributed origins (green) (Materials and methods) with two sets of parameter values: $L = 3000$ kb, $v = 0.6$ kb/min, $k_{on} = 1.2 \times 10^{-2}$ min^{-1} and $N_D^T = 12$ (dashed line) or 165 (solid line); (black diamonds) experimental data points for *Xenopus* embryo, *S. cerevisiae*, *S. cerevisae* grown in Hydroxyurea (HU), *S. pombe*, *D. melanogaster*, human (see text and ***Table 1***). The following figure supplement is available for ***Figure 2***.

DOI: https://doi.org/10.7554/eLife.35192.004

The following source data and figure supplement are available for figure 2:

Source data 1. Data file for the experimental *Xenopus* $I(t)$ in ***Figure 2 (a)***.

DOI: https://doi.org/10.7554/eLife.35192.006

Source data 2. Data file for the experimental *S.*

DOI: https://doi.org/10.7554/eLife.35192.007

Source data 3. Data file for the experimental parameters used in ***Figure 2 (c)***.

DOI: https://doi.org/10.7554/eLife.35192.008

Figure supplement 1. Different steps of the interaction between diffusing elements and origins of replication.

DOI: https://doi.org/10.7554/eLife.35192.005

this ratio is higher than one. For weak and moderate interactions (**Figure 1 (d)**, blue and green solid curves, respectively), this ratio stays bigger than one during all the S-phase, where $I_S(t)$ was shown to be monotonously increasing (**Figure 1 (b)**). For a strong interaction (**Figure 1 (b)**, red solid curve), this ratio reaches a maximum and then decreases below one, at a time corresponding to the maximum observed in $I_S(t)$ (**Figure 1 (d)**, red solid curve). Hence, the maximum of $I(t)$ corresponds to a switch of the balance between origin passivation and activation, the latter becoming predominant in late S-phase. We have seen that up to this maximum $\rho_{\mathrm{p-ori}}(t) \approx cte \approx \rho_0$, so $I_S(t) \approx k_{on}\rho_0 N_F(t)$. When $N_{FD}(t)$ reaches N^*_{FD}, then $I_S(t)$ reaches its maximum value:

$$I_{max} = k_{on}\rho_0 N^*_{FD} \approx \frac{\rho_0 v}{d(t)} \approx v\rho_0^2, \tag{5}$$

where we have used the approximation $d(t) \approx d(0) = 1/\rho_0$ (which is exact for periodically distributed *p-oris*). I_{max} can thus be predicted from two measurable parameters, providing a direct test of the model.

Comparison with different eukaryotes

Xenopus embryo

Given the huge size of *Xenopus* embryo chromosomes, to make the simulations more easily tractable, we rescaled the size L of the chromosomes, k_{on} and N_D^T to keep the duration of S-phase $T_{phase} \approx L/2vN_D^T$ and $I(t)$ (**Equation (2)**) unchanged ($L \to \alpha L$, $N_D^T \to \alpha N_D^T$, $k_{on} \to k_{on}/\alpha$). In **Figure 2 (a)** are reported the results of our simulations for a chromosome length $L = 3000$ kb. We see that a good agreement is obtained with experimental data (**Goldar et al., 2009**) when using either a uniform distribution of *p-oris* with a density $\rho_0 = 0.70$ kb^{-1} and a number of firing factors $N_D^T = 187$, or a periodic distribution with $\rho_0 = 0.28$ kb^{-1} and $N_D^T = 165$. A higher density of *p-oris* was needed for uniformly distributed *p-oris* where $d(t)$ (slightly) increases with time, than for periodically distributed *p-oris* where $d(t)$ fluctuates around a constant value $1/\rho_0$. The uniform distribution, which is the most natural to simulate *Xenopus* embryo replication, gives a density of activated origins of 0.17 kb^{-1} in good agreement with DNA combing data analysis (**Herrick et al., 2002**) but twice lower than estimated from real time replication imaging of surface-immobilized DNA in a soluble *Xenopus* egg extract system (**Loveland et al., 2012**). Note that in the latter work, origin licensing was performed in condition of incomplete chromatinization and replication initiation was obtained using a nucleoplasmic extract system with strong initiation activity, which may explain the higher density of activated origins observed in this work.

S. cerevisiae

To test the robustness of our minimal model with respect to the distribution of *p-oris*, we simulated the replication in *S. cerevisiae*, whose *p-oris* are known to be well positioned as reported in OriDB (**Siow et al., 2012**). 829 *p-oris* were experimentally identified and classified into three categories: Confirmed origins (410), Likely origins (216), and Dubious origins (203). When comparing the results obtained with our model to the experimental $I(t)$ data (**Goldar et al., 2009**) (**Figure 2 (b)**), we see that to obtain a good agreement we need to consider not only the Confirmed origins but also the Likely and the Dubious origins. This shows that in the context of our model, the number of *p-oris* required to reproduce the experimental $I(t)$ curve in *S. cerevisiae* exceeds the number of Confirmed and Likely origins. Apart from the unexpected activity of Dubious origins, the requirement for a larger number of origins can be met by some level of random initiation (**Czajkowsky et al., 2008**) or initiation events away from mapped origins due to helicase mobility (**Gros et al., 2015**; **Hyrien, 2016a**). If fork progression can push helicases along chromosomes instead of simply passivating them, there will be initiation events just ahead of progressing forks. Such events are not detectable by the replication profiling experiments used to determine $I(t)$ in **Figure 2(b)** and thus not accounted for by I_{max}. Given the uncertainty in replication fork velocity (a higher fork speed would require only Confirmed and Likely origins) and the possible experimental contribution of the *p-oris* in the rDNA part of chromosome 12 (not taken into account in our modeling), this conclusion needs to be confirmed in future experiments. It is to be noted that even if 829 *p-oris* are needed, on average only 352 origins have fired by the end of S-phase. For *S. cerevisiae* with well positioned *p-oris*, we have checked the robustness of our results with respect to a stochastic number of firing

factors N_D^T from cell to cell (Poisson distribution, ***Iyer-Biswas et al. (2009)***). We confirmed the $I(t)$ bell shape with a robust duration of the S-phase of 58.6 ± 4.3 min as compared to 58.5 ± 3.3 min obtained previously with a constant number of firing factors. Interestingly, in an experiment where hydroxyurea (HU) was added to the yeast growth media, the sequence of activation of replication origins was shown to be conserved even though T_{phase} was lengthened from 1 hr to 16 hr (***Alvino et al., 2007***). HU slows down the DNA synthesis to a rate of $\sim 50\,\mathrm{bp\ min^{-1}}$ corresponding to a 30-fold decrease of the fork speed (***Sogo et al., 2002***). Up to a rescaling of time, the replication kinetics of our model is governed by the ratio between replication fork speed and the productive-interaction rate k_{on} (neglecting here the possible contribution of the activation dynamics of firing factors). Hence, our model can capture the observation of ***Alvino et al. (2007)*** when considering a concomitant fork slowing down and k_{on} reduction in response to HU, which is consistent with the molecular action of the replication checkpoint induced by HU (***Zegerman and Diffley, 2010***). In a model where the increase of $I(t)$ results from the import of replication factors, the import rate would need to be reduced by the presence of HU in proportion with the lengthening of S-phase in order to maintain the pattern of origin activations. Extracting $I(t)$ from experimental replication data for cells grown in absence (HU^-) or presence (HU^+) (***Alvino et al., 2007***), we estimated $I_{max}^{HU-} \sim 6.0\,\mathrm{Mb^{-1}\,min^{-1}}$ and $I_{max}^{HU+} \sim 0.24\,\mathrm{Mb^{-1}\,min^{-1}}$ for HU^- and HU^+ cells, respectively. The ratio $I_{max}^{HU-}/I_{max}^{HU+} \simeq 24.8 \sim v^{HU-}/v^{HU+}$ is quite consistent with the prediction of the scaling law (***Equation (5)***) for a constant density of *p-oris*.

D. melanogaster and human

We gathered from the literature experimental estimates of I_{max}, ρ_0 and v for different eukaryotic organisms (***Table 1***). As shown in ***Figure 2 (c)***, when plotting I_{max} vs $v\rho_0^2$, all the experimental data points remarkably follow the diagonal trend indicating the validity of the scaling law (***Eq. (5)***) for all considered eukaryotes. We performed two series of simulations for fixed values of parameters k_o, N_D^T and v and decreasing values of ρ_0 with both periodic distribution (blue) and uniform (green) distributions of *p-oris* (***Figure 2 (c)***). The first set of parameters was chosen to cover high I_{max} values similar the one observed for *Xenopus* embryo (bullets, solid lines). When decreasing ρ_0, the number of firing factors becomes too large and $I(t)$ does no longer present a maximum. We thus decreased the value of N_D^T keeping all other parameters constant (boxes, dashed line) to explore smaller values of I_{max} in the range of those observed for human and *D. melanogaster*. We can observe that experimental data points' deviation from ***Equation (5)*** is smaller than the deviation due to specific *p-oris* distributions.

Table 1. Experimental data for various eukaryotic organisms with genome length L (Mb), replication fork velocity v (kb/min), number of *p-oris* ($N_{\mathrm{p-ori}}(t=0)$), $\rho_0 = N_{\mathrm{p-ori}}(t=0)/L$ ($\mathrm{kb^{-1}}$) and I_{max} ($\mathrm{Mb^{-1}min^{-1}}$).

All I_{max} data are from ***Goldar et al. (2009)***, except for *S. cerevisiae* grown in presence or absence of hydroxyurea (HU) which were computed from the replication profile of ***Alvino et al. (2007)***. For *S. cerevisiae* and *S. pombe*, Confirmed, Likely, and Dubious origins were taken into account. For *D. melanogaster*, $N_{\mathrm{p-ori}}(t=0)$ was obtained from the same Kc cell type as the one used to estimate I_{max}. For *Xenopus* embryo, we assumed that a *p-ori* corresponds to a dimer of MCM2-7 hexamer so that $N_{\mathrm{p-ori}}(t=0)$ was estimated as a half of the experimental density of MCM3 molecules reported for *Xenopus* sperm nuclei DNA in *Xenopus* egg extract (***Mahbubani et al., 1997***). For human, we averaged the number of origins experimentally identified in K562 (62971) and in MCF7 (94195) cell lines.

	L	v	$N_{\mathrm{p-ori}}$	ρ_0	I_{max}	Ref.
S. cerevisiae	12.5	1.60	829	0.066	6.0	***Sekedat et al. (2010)*** and ***Siow et al. (2012)***
S. cerevisiae in presence of HU	12.5	0.05	829	0.066	0.24	***Alvino et al. (2007)***. Same $N_{\mathrm{p-ori}}$ and ρ_0 as *S. cerevisiae* in normal growth condition.
S. pombe	12.5	2.80	741	0.059	10.0	***Siow et al. (2012)*** and ***Kaykov and Nurse (2015)***
D. melanogaster	143.6	0.63	6184	0.043	0.5	***Ananiev et al. (1977)*** and ***Cayrou et al. (2011)***
human	6469.0	1.46	78000	0.012	0.3	***Conti et al. (2007)*** and ***Martin et al. (2011)***
Xenopus sperm	2233.0	0.52	744333	0.333	70.0	***Mahbubani et al. (1997)*** and ***Loveland et al. (2012)***

DOI: https://doi.org/10.7554/eLife.35192.009

Note that in human it was suggested that early and late replicating domains could be modeled by spatial inhomogeneity of the *p-ori* distribution along chromosomes, with a high density in early replicating domains ($\rho_{0,early} = 2.6$ ORC/100 kb) and a low density in late replicating domains ($\rho_{0,late} = 0.2$ ORC/100 kb) (**Miotto et al., 2016**). If low- and high-density regions each cover one half of the genome and $\rho_{0,early} \gg \rho_{0,late}$, most *p-oris* are located in the high-density regions and the origin firing kinetics ($N_{fired}(t, t+dt)$) will mainly come from initiation in these regions. However, the length of unreplicated DNA also encompasses the late replicating domains resulting in a lowering of the global $I(t)$ by at least a factor of 2 (**Equation (1)**). Hence, in the context of our model $I_{max} \lesssim 0.5 v \rho_{early}^2$. Interestingly, considering the experimental values for the human genome ($I_{max} = 0.3\mathrm{Mb}^{-1}\mathrm{min}^{-1}$ and $v = 1.46\mathrm{kbmin}^{-1}$, **Table 1**), this leads to $\rho_{0,early} \gtrsim 2.3$ Ori/100 kb, in good agreement with the estimated density of 2.6 ORC/100 kb (**Miotto et al., 2016**). Inhomogeneities in origin density could create inhomogeneities in firing factor concentration that would further enhance the replication kinetics in high density regions, possibly corresponding to early replication foci.

Discussion

To summarize, we have shown that within the framework of 1D nucleation and growth models of DNA replication kinetics (**Herrick et al., 2002**; **Jun and Bechhoefer, 2005**), the sufficient conditions to obtain a universal bell shaped $I(t)$ as observed in eukaryotes are a strong bimolecular reaction between localized *p-oris* and limiting origin firing factors that travel with replication forks and are released at termination. Under these conditions, the density of *p-oris* naturally decreases by the end of the S-phase and so does $I_S(t)$. Previous models in *Xenopus* embryo (**Goldar et al., 2008**; **Gauthier and Bechhoefer, 2009**) assumed that all sites contained a *p-ori* implying that the time t_r to replicate DNA between two neighboring *p-oris* was close to zero. This clarifies why they needed some additional mechanisms to explain the final decrease of the firing rate. Moreover, our model predicts that the maximum value for $I(t)$ is intimately related to the density of *p-oris* and the fork speed (**Equation (5)**), and we have shown that without free parameter, this relationship holds for five species with up to a 300-fold difference of I_{max} and $v\rho_0^2$ (**Table 1**, **Figure 2 (c)**).

Our model assumes that all *p-oris* are governed by the same rule of initiation resulting from physicochemically realistic particulars of their interaction with limiting replication firing factors. Any spatial inhomogeneity in the firing rate $I(x,t)$ along the genomic coordinate in our simulations thus reflects the inhomogeneity in the distribution of the potential origins in the genome. In yeast, replication kinetics along chromosomes were robustly reproduced in simulations where each replication origin fires following a stochastic law with parameters that change from origin to origin (**Yang et al., 2010**). Interestingly, this heterogeneity between origins is captured by the Multiple-Initiator Model where origin firing time distribution is modeled by the number of MCM2-7 complexes bound at the origin (**Yang et al., 2010**; **Das et al., 2015**). In human, early and late replicating domains could be modeled by the spatial heterogeneity of the origin recognition complex (ORC) distribution (**Miotto et al., 2016**). In these models, MCM2-7 and ORC have the same status as our *p-oris*, they are potential origins with identical firing properties. Our results show that the universal bell-shaped temporal rate of replication origin firing can be explained irrespective of species-specific spatial heterogeneity in origin strength. Note, however, that current successful modeling of the chromosome organization of DNA replication timing relies on heterogeneities in origins' strength and spatial distributions (**Bechhoefer and Rhind, 2012**).

To confirm the simple physical basis of our modeling, we used molecular dynamics rules as previously developed for *S. cerevisiae* (**Arbona et al., 2017**) to simulate S-phase dynamics of chromosomes confined in a spherical nucleus. We added firing factors that are free to diffuse in the covolume left by the chain and that can bind to proximal *p-oris* to initiate replication, move along the chromosomes with the replication forks and be released when two fork merges. As shown in **Figure 2 (a,b)** for *Xenopus* embryo and *S. cerevisiae*, results confirmed the physical relevance of our minimal modeling and the validity of its predictions when the 3D diffusion of the firing factors is explicitly taken into account. Modeling of replication timing profiles in human was recently successfully achieved in a model with both inhibition of origin firing 55 kb around active forks, and an enhanced firing rate further away up to a few 100 kb (**Löb et al., 2016**) as well as in models that do not consider any inhibition nor enhanced firing rate due to fork progression (**Gindin et al., 2014**;

Miotto et al., 2016). These works illustrate that untangling spatio-temporal correlations in replication kinetics is challenging. 3D modeling opens new perspectives for understanding the contribution of firing factor transport to the correlations between firing events along chromosomes. For example in *S. cerevisiae* (*Knott et al., 2012*) and in *S. pombe* (*Kaykov and Nurse, 2015*), a higher firing rate has been reported near origins that have just fired (but see *Yang et al. (2010)*). In mammals, megabase chromosomal regions of synchronous firing were first observed a long time ago (*Huberman and Riggs, 1968*; *Hyrien, 2016b*) and the projection of the replication program on 3D models of chromosome architecture was shown to reproduce the observed S-phase dynamics of replication foci (*Löb et al., 2016*). Recently, profiling of replication fork directionality obtained by Okazaki fragment sequencing have suggested that early firing origins located at the border of Topologically Associating Domains (TADs) trigger a cascade of secondary initiation events propagating through the TAD (*Petryk et al., 2016*). Early and late replicating domains were associated with nuclear compartments of open and closed chromatin (*Ryba et al., 2010*; *Boulos et al., 2015*; *Goldar et al., 2016*; *Hyrien, 2016b*). In human, replication timing U-domains (0.1–3 Mb) were shown to correlate with chromosome structural domains (*Baker et al., 2012*; *Moindrot et al., 2012*; *Pope et al., 2014*) and chromatin loops (*Boulos et al., 2013*, *Boulos et al., 2014*).

Understanding to which extent spatio-temporal correlations of the replication program can be explained by the diffusion of firing factors in the tertiary chromatin structure specific to each eukaryotic organism is a challenging issue for future work.

Materials and methods

Well-mixed model simulations

Each model simulation allows the reconstruction of the full replication kinetics during one S-phase. Chromosome initial replication state is described by the distribution of *p-oris* along each chromosomes. For *Xenopus* embryo, *p-ori* positions are randomly determined at the beginning of each simulation following two possible scenarios:

- For the uniform distribution scenario, $L\rho_0$ origins are randomly positions in the segment $[0, L]$, where ρ_0 is the average density of potential origins and L the total length of DNA.
- For the periodic distribution scenario, exactly one origin is positioned in every non-overlapping $1/\rho_0$ long segment. Within each segment, the position of the origin is chosen randomly in order to avoid spurious synchronization effects.

For yeast, the *p-ori* positions are identical in each S-phase simulations and correspond to experimentally determined positions reported in OriDB (*Siow et al., 2012*). The simulation starts with a fixed number N_D^T of firing factors that are progressively made available as described in Results. At every time step $t = ndt$, each free firing factor (available factors not bound to an active replication fork) has a probability to fire one of the $N_{p-ori}(t)$ *p-oris* at unreplicated loci given by:

$$1 - (1 - k_{on}dt)^{N_{p-ori}(t)}. \tag{6}$$

A random number is generated, and if it is inferior to this probability, an unreplicated *p-ori* is chosen at random, two diverging forks are created at this locus and the number of free firing factors decreases by 1. Finally, every fork is propagated by a length vdt resulting in an increase amount of DNA marked as replicated and possibly to the passivation of some *p-oris*. If two forks meet they are removed and the number of free firing factors increases by 1. Forks that reach the end of a chromosome are discarded. The numbers of firing events ($N_{fired}(t)$), origin passivations, free firing factors ($N_{FD}(t)$) and unreplicated *p-oris* ($N_{\mathrm{p-ori}}(t)$) as well as the length of unreplicated DNA ($L_{unrepDNA}(t)$) are recorded allowing the computation of $I_S(t)$ (*Eq. (1)*), the normalized density of *p-oris* ($\rho_{\mathrm{p-ori}}(t))/\rho_0$), the normalized number of free firing factors ($N_{FD}(t)/N^*_{FD}(t)$) and the ratio between the number of origin passivations and activations. Simulation ends when all DNA has been replicated, which define the replication time.

3D model simulations

Replication kinetics simulation for the 3D model follows the same steps as in the well-mixed model except that the probability that a free firing factor activates an unreplicated *p-ori* depends on their

distance d obtained from a molecular dynamic simulation performed in parallel to the replication kinetics simulation. We used HOOMD-blue (**Anderson et al., 2008**) with parameters similar to the ones previously considered in **Arbona et al. (2017)** to simulate chromosome conformation dynamics and free firing factor diffusion within a spherical nucleus of volume V_N. The details of the interaction between the diffusing firing factors and the *p-oris* is illustrated in **Figure 2—figure supplement 1**. Given a capture radius r_c set to two coarse grained chromatin monomer radiuses, when a free firing factor is within the capture volume $V_c = \frac{4}{3}\pi r_c^3$ around an unreplicated *p-ori* ($d<r_c$), it can activate the origin with a probability p. In order to have a similar firing activity as in the well-mixed model, r_c and p were chosen so that pV_c/V_N takes a value comparable to the k_{on} values used in the well-mixed simulations.

For each set of parameters of the well-mixed and 3D models, we reported the mean curves obtained over a number of independent simulations large enough so that the noisy fluctuations of the mean $I_S(t)$ are small compared to the average bell-shaped curve. The complete set of parameters for each simulation series is provided in **Supplementary file 1**. The scripts used to extract yeast $I(t)$ from the experimental data of **Alvino et al. (2007)** can be found here https://github.com/ jeammimi/ifromprof/blob/master/notebooks/exploratory/Alvino_WT.ipynb (yeast in normal growth conditions) and here https://github.com/jeammimi/ifromprof/blob/master/notebooks/exploratory/Alvino_H.ipynb (yeast grown grown in Hydroxyurea) (**Arbona and Goldar, 2018**). A copy is archived at https://github.com/elifesciences-publications/ifromprof.

Acknowledgements

We thank F. Argoul for helpful discussions. This work was supported by Institut National du Cancer (PLBIO16-302), Fondation pour la Recherche Médicale (DEI20151234404) and Agence Nationale de la Recherche (ANR-15-CE12-0011-01). BA acknowledges support from Science and Technology Commission of Shanghai Municipality (15520711500) and Joint Research Institute for Science and Society (JoRISS). We gratefully acknowledge support from the PSMN (Pôle Scientifique de Modélisation Numérique) of the ENS de Lyon for the computing resources. We thank BioSyL Federation and Ecofect LabEx (ANR-11-LABX-0048) for inspiring scientific events.

Additional information

Funding

Funder	Grant reference number	Author
Institut National Du Cancer	PLBIO16-302	Olivier Hyrien Benjamin Audit
Fondation pour la Recherche Médicale	DEI20151234404	Arach Goldar Olivier Hyrien Benjamin Audit
Agence Nationale de la Recherche	ANR-15-CE12-0011-01	Olivier Hyrien Alain Arneodo Benjamin Audit
Joint Research Institute for Science and Society	JoRISS 2017-2018	Benjamin Audit

The funders had no role in study design, data collection and interpretation, or the decision to submit the work for publication.

Author contributions

Jean-Michel Arbona, Data curation, Software, Formal analysis, Investigation, Visualization, Methodology, Writing—original draft, Writing—review and editing; Arach Goldar, Conceptualization, Resources, Data curation, Validation, Methodology; Olivier Hyrien, Benjamin Audit, Conceptualization, Supervision, Funding acquisition, Validation, Writing—original draft, Writing—review and editing; Alain Arneodo, Conceptualization, Supervision, Writing—original draft, Writing—review and editing

Author ORCIDs
Jean-Michel Arbona http://orcid.org/0000-0001-6166-9056
Olivier Hyrien http://orcid.org/0000-0001-8879-675X
Benjamin Audit http://orcid.org/0000-0003-2683-9990

Decision letter and Author response
Decision letter https://doi.org/10.7554/eLife.35192.013
Author response https://doi.org/10.7554/eLife.35192.014

Additional files

Supplementary files

- Supplementary file 1. This file provides: the parameter values used for all the simulations in ***Figures 1*** and ***2***; the list of all the symbols used in the main text and their meanings.
DOI: https://doi.org/10.7554/eLife.35192.010
- Transparent reporting form
DOI: https://doi.org/10.7554/eLife.35192.011

Data availability

All experimental data analyzed in this study are included in the manuscript. Source data files have been provided for Figure 2.

References

Alvino GM, Collingwood D, Murphy JM, Delrow J, Brewer BJ, Raghuraman MK. 2007. Replication in hydroxyurea: it's a matter of time. *Molecular and Cellular Biology* **27**:6396–6406. DOI: https://doi.org/10.1128/MCB.00719-07, PMID: 17636020

Ananiev EV, Polukarova LG, Yurov YB. 1977. Replication of chromosomal DNA in diploid *Drosophila melanogaster* cells cultured in vitro. *Chromosoma* **59**:259–272. DOI: https://doi.org/10.1007/BF00292782, PMID: 138582

Anderson JA, Lorenz CD, Travesset A. 2008. General purpose molecular dynamics simulations fully implemented on graphics processing units. *Journal of Computational Physics* **227**:5342–5359. DOI: https://doi.org/10.1016/j.jcp.2008.01.047

Araki H. 2016. Elucidating the DDK-dependent step in replication initiation. *The EMBO Journal* **35**:907–908. DOI: https://doi.org/10.15252/embj.201694227, PMID: 27006277

Arbona JM, Goldar A. 2018. *GitHub*. 790e325. https://github.com/jeammimi/ifromprof/

Arbona JM, Herbert S, Fabre E, Zimmer C. 2017. Inferring the physical properties of yeast chromatin through Bayesian analysis of whole nucleus simulations. *Genome Biology* **18**:81. DOI: https://doi.org/10.1186/s13059-017-1199-x, PMID: 28468672

Baker A, Audit B, Chen CL, Moindrot B, Leleu A, Guilbaud G, Rappailles A, Vaillant C, Goldar A, Mongelard F, d'Aubenton-Carafa Y, Hyrien O, Thermes C, Arneodo A. 2012. Replication fork polarity gradients revealed by megabase-sized U-shaped replication timing domains in human cell lines. *PLoS Computational Biology* **8**:e1002443. DOI: https://doi.org/10.1371/journal.pcbi.1002443, PMID: 22496629

Bechhoefer J, Marshall B. 2007. How Xenopus laevis replicates DNA reliably even though its origins of replication are located and initiated stochastically. *Physical Review Letters* **98**:098105. DOI: https://doi.org/10.1103/PhysRevLett.98.098105, PMID: 17359202

Bechhoefer J, Rhind N. 2012. Replication timing and its emergence from stochastic processes. *Trends in Genetics* **28**:374–381. DOI: https://doi.org/10.1016/j.tig.2012.03.011, PMID: 22520729

Boulos RE, Arneodo A, Jensen P, Audit B. 2013. Revealing long-range interconnected hubs in human chromatin interaction data using graph theory. *Physical Review Letters* **111**:118102. DOI: https://doi.org/10.1103/PhysRevLett.111.118102, PMID: 24074120

Boulos RE, Drillon G, Argoul F, Arneodo A, Audit B. 2015. Structural organization of human replication timing domains. *FEBS Letters* **589**:2944–2957. DOI: https://doi.org/10.1016/j.febslet.2015.04.015, PMID: 25912651

Boulos RE, Julienne H, Baker A, Chen C-L, Petryk N, Kahli M, d'Aubenton-Carafa Y, Goldar A, Jensen P, Hyrien O, Thermes C, Arneodo A, Audit B. 2014. From the chromatin interaction network to the organization of the human genome into replication N/U-domains. *New Journal of Physics* **16**:115014. DOI: https://doi.org/10.1088/1367-2630/16/11/115014

Cayrou C, Coulombe P, Vigneron A, Stanojcic S, Ganier O, Peiffer I, Rivals E, Puy A, Laurent-Chabalier S, Desprat R, Méchali M. 2011. Genome-scale analysis of metazoan replication origins reveals their organization in specific but flexible sites defined by conserved features. *Genome Research* **21**:1438–1449. DOI: https://doi.org/10.1101/gr.121830.111, PMID: 21750104

Conti C, Saccà B, Herrick J, Lalou C, Pommier Y, Bensimon A. 2007. Replication fork velocities at adjacent replication origins are coordinately modified during DNA replication in human cells. *Molecular Biology of the Cell* **18**:3059–3067. DOI: https://doi.org/10.1091/mbc.e06-08-0689, PMID: 17522385

Czajkowsky DM, Liu J, Hamlin JL, Shao Z. 2008. DNA combing reveals intrinsic temporal disorder in the replication of yeast chromosome VI. *Journal of Molecular Biology* **375**:12–19. DOI: https://doi.org/10.1016/j.jmb.2007.10.046, PMID: 17999930

Das SP, Borrman T, Liu VWT, Yang SC-H, Bechhoefer J, Rhind N. 2015. Replication timing is regulated by the number of MCMs loaded at origins. *Genome Research* **25**:1886–1892. DOI: https://doi.org/10.1101/gr.195305.115

de Moura AP, Retkute R, Hawkins M, Nieduszynski CA. 2010. Mathematical modelling of whole chromosome replication. *Nucleic Acids Research* **38**:5623–5633. DOI: https://doi.org/10.1093/nar/gkq343, PMID: 20457753

Gauthier MG, Bechhoefer J. 2009. Control of DNA replication by anomalous reaction-diffusion kinetics. *Physical Review Letters* **102**:158104. DOI: https://doi.org/10.1103/PhysRevLett.102.158104, PMID: 19518676

Gindin Y, Valenzuela MS, Aladjem MI, Meltzer PS, Bilke S. 2014. A chromatin structure-based model accurately predicts DNA replication timing in human cells. *Molecular Systems Biology* **10**:722. DOI: https://doi.org/10.1002/msb.134859, PMID: 24682507

Goldar A, Arneodo A, Audit B, Argoul F, Rappailles A, Guilbaud G, Petryk N, Kahli M, Hyrien O. 2016. Deciphering DNA replication dynamics in eukaryotic cell populations in relation with their averaged chromatin conformations. *Scientific Reports* **6**:22469. DOI: https://doi.org/10.1038/srep22469, PMID: 26935043

Goldar A, Labit H, Marheineke K, Hyrien O. 2008. A dynamic stochastic model for DNA replication initiation in early embryos. *PLoS One* **3**:e2919. DOI: https://doi.org/10.1371/journal.pone.0002919, PMID: 18682801

Goldar A, Marsolier-Kergoat MC, Hyrien O. 2009. Universal temporal profile of replication origin activation in eukaryotes. *PLoS One* **4**:e5899. DOI: https://doi.org/10.1371/journal.pone.0005899, PMID: 19521533

Gros J, Kumar C, Lynch G, Yadav T, Whitehouse I, Remus D. 2015. Post-licensing specification of eukaryotic replication origins by facilitated Mcm2-7 sliding along DNA. *Molecular Cell* **60**:797–807. DOI: https://doi.org/10.1016/j.molcel.2015.10.022, PMID: 26656162

Hawkins M, Retkute R, Müller CA, Saner N, Tanaka TU, de Moura AP, Nieduszynski CA. 2013. High-resolution replication profiles define the stochastic nature of genome replication initiation and termination. *Cell Reports* **5**:1132–1141. DOI: https://doi.org/10.1016/j.celrep.2013.10.014, PMID: 24210825

Herrick J, Jun S, Bechhoefer J, Bensimon A. 2002. Kinetic model of DNA replication in eukaryotic organisms. *Journal of Molecular Biology* **320**:741–750. DOI: https://doi.org/10.1016/S0022-2836(02)00522-3, PMID: 12095252

Huberman JA, Riggs AD. 1968. On the mechanism of DNA replication in mammalian chromosomes. *Journal of Molecular Biology* **32**:327–341. DOI: https://doi.org/10.1016/0022-2836(68)90013-2, PMID: 5689363

Hyrien O, Goldar A. 2010. Mathematical modelling of eukaryotic DNA replication. *Chromosome Research* **18**:147–161. DOI: https://doi.org/10.1007/s10577-009-9092-4, PMID: 20205354

Hyrien O, Marheineke K, Goldar A. 2003. Paradoxes of eukaryotic DNA replication: MCM proteins and the random completion problem. *BioEssays* **25**:116–125. DOI: https://doi.org/10.1002/bies.10208, PMID: 12539237

Hyrien O, Rappailles A, Guilbaud G, Baker A, Chen CL, Goldar A, Petryk N, Kahli M, Ma E, d'Aubenton-Carafa Y, Audit B, Thermes C, Arneodo A. 2013. From simple bacterial and archaeal replicons to replication N/U-domains. *Journal of Molecular Biology* **425**:4673–4689 . DOI: https://doi.org/10.1016/j.jmb.2013.09.021, PMID: 24095859

Hyrien O. 2016a. How MCM loading and spreading specify eukaryotic DNA replication initiation sites. *F1000Research* **5**:2063. DOI: https://doi.org/10.12688/f1000research.9008.1

Hyrien O. 2016b. Up and down the slope: Replication timing and fork directionality gradients in eukaryotic genomes. In: Kaplan D. L (Ed). *The Initiation of DNA Replication in Eukaryotes* . Switzerland: Springer International Publishing. p. 65–85.

Iyer-Biswas S, Hayot F, Jayaprakash C. 2009. Stochasticity of gene products from transcriptional pulsing. *Physical Review E* **79**:031911. DOI: https://doi.org/10.1103/PhysRevE.79.031911

Jun S, Bechhoefer J. 2005. Nucleation and growth in one dimension. II. application to DNA replication kinetics. *Physical Review E* **71**:011909. DOI: https://doi.org/10.1103/PhysRevE.71.011909

Kaykov A, Nurse P. 2015. The spatial and temporal organization of origin firing during the S-phase of fission yeast. *Genome Research* **25**:391–401. DOI: https://doi.org/10.1101/gr.180372.114, PMID: 25650245

Knott SR, Peace JM, Ostrow AZ, Gan Y, Rex AE, Viggiani CJ, Tavaré S, Aparicio OM. 2012. Forkhead transcription factors establish origin timing and long-range clustering in *S. cerevisiae*. *Cell* **148**:99–111. DOI: https://doi.org/10.1016/j.cell.2011.12.012, PMID: 22265405

Loveland AB, Habuchi S, Walter JC, van Oijen AM. 2012. A general approach to break the concentration barrier in single-molecule imaging. *Nature Methods* **9**:987–992. DOI: https://doi.org/10.1038/nmeth.2174, PMID: 22961247

Löb D, Lengert N, Chagin VO, Reinhart M, Casas-Delucchi CS, Cardoso MC, Drossel B. 2016. 3D replicon distributions arise from stochastic initiation and domino-like DNA replication progression. *Nature Communications* **7**:11207. DOI: https://doi.org/10.1038/ncomms11207, PMID: 27052359

Machida YJ, Hamlin JL, Dutta A. 2005. Right place, right time, and only once: replication initiation in metazoans. *Cell* **123**:13–24. DOI: https://doi.org/10.1016/j.cell.2005.09.019, PMID: 16213209

Mahbubani HM, Chong JP, Chevalier S, Thömmes P, Blow JJ. 1997. Cell cycle regulation of the replication licensing system: involvement of a Cdk-dependent inhibitor. *The Journal of Cell Biology* **136**:125–135. DOI: https://doi.org/10.1083/jcb.136.1.125, PMID: 9008708

Martin MM, Ryan M, Kim R, Zakas AL, Fu H, Lin CM, Reinhold WC, Davis SR, Bilke S, Liu H, Doroshow JH, Reimers MA, Valenzuela MS, Pommier Y, Meltzer PS, Aladjem MI. 2011. Genome-wide depletion of replication initiation events in highly transcribed regions. *Genome Research* **21**:1822–1832. DOI: https://doi.org/10.1101/gr.124644.111

Miotto B, Ji Z, Struhl K. 2016. Selectivity of ORC binding sites and the relation to replication timing, fragile sites, and deletions in cancers. *PNAS* **113**:E4810–E4819. DOI: https://doi.org/10.1073/pnas.1609060113, PMID: 27436900

Moindrot B, Audit B, Klous P, Baker A, Thermes C, de Laat W, Bouvet P, Mongelard F, Arneodo A. 2012. 3D chromatin conformation correlates with replication timing and is conserved in resting cells. *Nucleic Acids Research* **40**:9470–9481. DOI: https://doi.org/10.1093/nar/gks736, PMID: 22879376

Petryk N, Kahli M, d'Aubenton-Carafa Y, Jaszczyszyn Y, Shen Y, Silvain M, Thermes C, Chen CL, Hyrien O. 2016. Replication landscape of the human genome. *Nature Communications* **7**:10208. DOI: https://doi.org/10.1038/ncomms10208, PMID: 26751768

Pope BD, Ryba T, Dileep V, Yue F, Wu W, Denas O, Vera DL, Wang Y, Hansen RS, Canfield TK, Thurman RE, Cheng Y, Gülsoy G, Dennis JH, Snyder MP, Stamatoyannopoulos JA, Taylor J, Hardison RC, Kahveci T, Ren B, et al. 2014. Topologically associating domains are stable units of replication-timing regulation. *Nature* **515**:402–405. DOI: https://doi.org/10.1038/nature13986, PMID: 25409831

Ryba T, Hiratani I, Lu J, Itoh M, Kulik M, Zhang J, Schulz TC, Robins AJ, Dalton S, Gilbert DM. 2010. Evolutionarily conserved replication timing profiles predict long-range chromatin interactions and distinguish closely related cell types. *Genome Research* **20**:761–770. DOI: https://doi.org/10.1101/gr.099655.109, PMID: 20430782

Sekedat MD, Fenyö D, Rogers RS, Tackett AJ, Aitchison JD, Chait BT. 2010. GINS motion reveals replication fork progression is remarkably uniform throughout the yeast genome. *Molecular Systems Biology* **6**:353. DOI: https://doi.org/10.1038/msb.2010.8, PMID: 20212525

Siow CC, Nieduszynska SR, Müller CA, Nieduszynski CA, OriDB NCA. 2012. OriDB, the DNA replication origin database updated and extended. *Nucleic Acids Research* **40**:D682–D686. DOI: https://doi.org/10.1093/nar/gkr1091, PMID: 22121216

Sogo JM, Lopes M, Foiani M. 2002. Fork reversal and ssDNA accumulation at stalled replication forks owing to checkpoint defects. *Science* **297**:599–602. DOI: https://doi.org/10.1126/science.1074023, PMID: 12142537

Yang SC, Rhind N, Bechhoefer J. 2010. Modeling genome-wide replication kinetics reveals a mechanism for regulation of replication timing. *Molecular Systems Biology* **6**:404. DOI: https://doi.org/10.1038/msb.2010.61, PMID: 20739926

Yang SC-H, Bechhoefer J. 2008. How *Xenopus laevis* embryos replicate reliably: Investigating the random-completion problem . *Physical Review E* **78**:041917. DOI: https://doi.org/10.1103/PhysRevE.78.041917

Zegerman P, Diffley JF. 2010. Checkpoint-dependent inhibition of DNA replication initiation by Sld3 and Dbf4 phosphorylation. *Nature* **467**:474–478. DOI: https://doi.org/10.1038/nature09373, PMID: 20835227